Pergamon

Int. J. Solids Structures Vol. 33, No. 8, pp. 1191–1207, 1996

0020-7683/96 $15.00 + .00

0020-7683(95)00066-6

FINITE ELEMENT SIMULATION OF MODE I DYNAMIC, DUCTILE FRACTURE INITIATION

SUMIT BASU and R. NARASIMHAN
Department of Mechanical Engineering, Indian Institute of Science, Bangalore 560012, India

(*Received* 7 *July* 1994; *in revised form* 10 *March* 1995)

Abstract—In this work, two-dimensional (plane strain) finite element analysis of a ductile three-point bend fracture specimen subjected to mode I quasi-static and dynamic (impact-like) loading is conducted. The Gurson constitutive model that accounts for the ductile failure mechanisms of micro-void nucleation, growth and coalescence is employed within the framework of a finite deformation plasticity theory. The interaction between the notch tip and a pre-nucleated hole ahead of it is modelled. Several dynamic analyses are performed considering rate-independent and rate-dependent material behaviour and with different impact speeds. The development of ductile failure is studied by monitoring the growth of the hole and the accumulation of the micro-void damage in the ligament between the hole and the notch tip. It is observed from the above analyses that though the effect of inertia on dynamic, ductile fracture initiation is moderate, strain rate sensitivity has a strong effect on many aspects of this phenomenon.

1. INTRODUCTION

Ductile fracture occurs on the micro-scale by nucleation, growth and coalescence of voids. The nucleation of voids occurs mainly by brittle cracking or interfacial decohesion of inclusions. This is followed by growth of the voids which is caused by plastic deformation in the surrounding material and is strongly influenced by high triaxial tension. It has been observed [see, for example, Cox and Low (1974)] that in structural materials such as steels and aluminium alloys void initiation can involve two distinct populations of inclusions. In such materials, voids initiate first at larger inclusions, and after growing to some size, they coalesce, or link up with a nearby crack tip via a void sheet consisting of voids nucleated from smaller particles.

Several studies have been undertaken to model the micro-mechanics of ductile fracture. In an early investigation, Rice and Johnson (1970) studied the growth of a void lying directly ahead of a crack tip due to the intense deformation fields generated by the blunting of the crack tip. In their model, fracture initiation is assumed to occur when the void has grown to a size such that its maximum dimension is equal to the width of the ligament connecting the crack tip and the void. They employed a slip line field analysis that accounted for finite geometry change in conjunction with the results of Rice and Tracey (1969) for the growth of an isolated spherical void and predicted the critical crack tip opening displacement at fracture initiation as a function of inclusion size and spacing. McMeeking (1977) conducted a similar investigation but used a finite element procedure that modelled large geometry changes. He examined the growth of voids located either directly ahead of the tip or at an angle of 45° following crack blunting.

In recent years, several investigators have employed a local approach in which damage accumulation models like the Gurson (1977) model were used to study ductile failure under various situations. Tvergaard and Needleman (1984) analysed cup and cone fracture in a round tensile bar. Aoki *et al.* (1984) and Aravas and McMeeking (1985) examined the interaction between a crack tip and a void. The presence of small-scale voids was accounted for in these studies by using the Gurson model. Needleman and Tvergaard (1987) studied quasi-static fracture initiation in a ductile material having two sets of inclusions of different sizes. The nucleation of voids at these inclusions was represented within the framework of the Gurson model.

The fracture mechanics concepts employed for designing structural components are generally based on the static fracture toughness K_{Ic}. However, in many engineering applications, highly dynamic loading may be encountered. This includes failure of metallic armour by projectile impact, explosive detonation, pressurized thermal shocks in nuclear reactors, etc. For many metallic materials, the dynamic fracture toughness K_{Id} depends strongly on the loading rate $\dot{K}$. In certain materials, it has been found (Priest, 1976) that K_{Id} decreases as $\dot{K}$ increases within nominal rates. This phenomenon increases the risk of fracture when such materials are subjected to dynamic loading. Hence, it is imperative to conduct a detailed study of the mechanisms operative in the micro-scale which lead to ductile fracture initiation and propagation under dynamic loading conditions. In particular, it is important to identify the factors pertaining to the material behaviour (such as, material inertia and strain rate sensitivity) which are responsible for causing different trends in the variation of the dynamic (ductile) fracture toughness with loading rate (Priest, 1976). An understanding of these effects will help in developing materials which will be better suited to resist dynamic fracture.

The studies reported in the literature on ductile fracture initiation under dynamic loading using damage accumulation models have not been as extensive as for quasi-static fracture initiation. Such an approach holds the key to an understanding of the effects of the factors mentioned above in dynamic ductile fracture initiation. Tvergaard and Needleman (1988) performed a dynamic finite element analysis of the Charpy impact test to investigate ductile–brittle transition of a high nitrogen steel. Needleman and Tvergaard (1991) simulated dynamic crack propagation in a ductile material containing two populations of second-phase particles. The modelling approach adopted in this work was similar to the earlier study of Needleman and Tvergaard (1987). Jha and Narasimhan (1992) conducted a transient finite element analysis of a three-point bend specimen of AISI 4340 steel under drop-weight impact loading. This study showed that the evolution of micro-mechanical quantities such as matrix plastic strain and void volume fraction near the notch root correlated closely with the time variation of the dynamic J integral, J_d (Nakamura *et al.*, 1986). This important result establishes the basis for the use of J to characterize ductile fracture initiation under transient loading. Benson (1993) investigated the effects of void distribution on coalescence patterns under dynamic loading.

The aim of the present work is to simulate ductile failure via the Gurson model and to assess quantitatively the effects of inertia and strain rate sensitivity on dynamic fracture initiation. As noted already, many engineering materials contain a dual population of void nucleating particles. Narasimhan and Kamat (1994) conducted a preliminary study with the above-mentioned objective and simulated a ductile material with two sets of void nucleating particles using an approach similar to that of Needleman and Tvergaard (1987). The methodology adopted in the present work is more realistic and is akin to the work of Aravas and McMeeking (1985) for quasi-static fracture initiation. Here, a ductile three-point bend fracture specimen with a pre-nucleated large size hole ahead of the notch tip is considered. The background material is represented using the Gurson model and strain controlled micro-void nucleation at uniformly distributed small particles is accounted for within the framework of the constitutive equations. Finite element analyses (two-dimensional plane strain) of the specimen subjected to both mode I, quasi-static and dynamic (impact-like) loading are conducted. Several dynamic analyses are performed considering rate-independent and rate-dependent material response and with different impact speeds. The computations are carried out until the stage when the entire ligament connecting the notch tip and the hole experiences failure by micro-void coalescence. From the results of the above analyses, the growth of the hole near the notch tip and the accumulation of micro-void damage in the ligament connecting them are studied and the effects of inertia and strain rate sensitivity are assessed.

2. CONSTITUTIVE MODEL

In this work, the viscoplastic version of the Gurson constitutive model, which was introduced by Pan *et al.* (1983), is employed. This model characterizes porosity in the

material in terms of a single internal variable f, the void volume fraction. The viscoplastic potential function depends on the macroscopic (aggregate) Cauchy stress tensor σ_{ij}, the matrix (microscopic) tensile flow stress σ_m and the void volume f, and is given by:

$$\Phi(\sigma_{ij},\sigma_m,f)=\frac{\sigma_e^2}{\sigma_m^2}+2f^*q_1\cosh\left(\frac{3\sigma_H}{2\sigma_m}\right)-(1+(q_1f^*)^2)=0. \tag{1}$$

Here, σ_m is the tensile flow strength of the matrix material. The macroscopic equivalent stress σ_e and the hydrostatic stress σ_H are defined by,

$$\sigma_e=\sqrt{(\tfrac{3}{2}S_{ij}S_{ij})}$$

and

$$\sigma_H=\tfrac{1}{3}\sigma_{kk}, \tag{2}$$

where $S_{ij}=\sigma_{ij}-\sigma_H\delta_{ij}$ is the stress deviator.

The parameter q_1 in eqn (1) was introduced by Tvergaard (1981, 1982), with a suggested value of 1.5, to obtain better agreement between the predictions of the above model and numerical studies on periodic array of voids. The function $f^*(f)$ was proposed by Tvergaard and Needleman (1984) to account for rapid evolution of f due to void coalescence near failure and is given by:

$$f^*=\begin{cases}f & f\leqslant f_c\\ f_c+K(f-f_c) & f>f_c,\end{cases} \tag{3}$$

where $K=(1/q_1-f_c)/(f_F-f_c)$. Here, f_c is the value of the void volume fraction at which void coalescence commences and f_F is its value at final failure. From eqns (1) and (3), it is evident that as $f\to f_F$, $f^*\to f_u^*=1/q_1$ and the material loses all its stress carrying capacity. Thus, an essential feature of this model is that a failure criterion is built directly into the constitutive equations. An estimate of f_c obtained by Brown and Embury (1973) from a simple model is 0.15. Also, a numerical investigation by Andersson (1977) suggests that $f_F\approx 0.25$.

In general, the evolution of the void volume fraction is due to growth of existing voids as well as due to nucleation of new voids and hence

$$\dot f=\dot f_{\text{growth}}+\dot f_{\text{nucleation}}. \tag{4}$$

The growth law, which is described by

$$\dot f_{\text{growth}}=(1-f)D^p_{kk}, \tag{5}$$

is an outcome of the plastic incompressibility of the matrix material. In this work, a plastic strain controlled void nucleation law is used to model micro-void nucleation at small particles (less than, say, 1 μm in size), as suggested by Thomason (1990), which are assumed to be uniformly distributed in the matrix. Thus,

$$\dot f_{\text{nucleation}}=\mathcal{A}\dot\varepsilon^p_m, \tag{6}$$

where, $\mathcal{A}(\cdot)$ is a function of the matrix plastic strain ε^p_m. The function $\mathcal{A}(\varepsilon^p_m)$ is chosen as (Chu and Needleman, 1980)

$$\mathscr{A} = \frac{f_n}{s_n\sqrt{2\pi}}\exp\left[-\frac{1}{2}\left(\frac{\varepsilon_m^p - \varepsilon_n}{s_n}\right)^2\right], \tag{7}$$

so that void nucleation follows a normal distribution about a mean nucleation strain ε_n and with a standard deviation s_n. In the above equation, f_n denotes the volume fraction of the uniformly distributed small particles. In addition, a pre-nucleated large void (comparable in size with the initial notch diameter) ahead of the notch tip will be considered (see Section 3). The actual process of initiation of this large void by interfacial decohesion around a second-phase particle (Argon *et al.*, 1975) is not modelled in this work.

The matrix material is characterized as a viscoplastic solid (i.e. one that displays flow stress elevation at high strain rates) and the matrix plastic strain rate $\dot{\varepsilon}_m^p$ is given by:

$$\dot{\varepsilon}_m^p = \dot{\varepsilon}_0\left(\frac{\sigma_m}{g(\varepsilon_m^p)}\right)^{1/m}. \tag{8}$$

Here, $\dot{\varepsilon}_0$ is a reference strain rate and m is a rate exponent. The function $g(\varepsilon_m^p)$ represents the effective tensile flow stress of the matrix material in a tensile test carried out at a strain rate such that $\dot{\varepsilon}_m^p = \dot{\varepsilon}_0$. In this work, an isotropic power law hardening material with a strain hardening exponent N is considered, so that

$$g(\varepsilon_m^p) = \sigma_0\left(\frac{\varepsilon_m^p}{\varepsilon_0} + 1\right)^N. \tag{9}$$

Here, σ_0 is the initial yield stress and $\varepsilon_0 = \sigma_0/E$, E being the Young's modulus, is the yield strain. It should be noted from eqn (8) that in the limit as the strain rate exponent $m \to 0$, the present viscoplastic material model reduces to the rate-independent Gurson model. Thus, the modelling of slow, quasi-static loading (when the viscoplastic material will not display any flow stress elevation) as well as rate-independent behaviour under dynamic loading can be accomplished by using a very small value for m, as will be mentioned in Section 3.

Equations (1)–(7) are used within the framework of a finite deformation elastic–viscoplastic theory with small elastic strains [see, for example, Needleman and Tvergaard (1987)]. The final constitutive equations are derived by following the rate tangent modulus method proposed by Pierce *et al.* (1984).

As noted earlier, complete loss of material stress carrying capacity occurs when $f^* = f_u^* = 1/q_1$ (or equivalently when $f = f_F$) resulting in local material failure. This implies that the material completely separates at this point and a traction-free surface develops. This failure criterion was implemented in the numerical simulation by freezing the evolution of f after it reaches a value close to f_F (around $0.95f_F$). The macroscopic material response is then elastic–perfectly plastic with a small pressure-dependent yield stress. The condition $f = 0.95f_F$ was used instead of $f = f_F$, because as $f \to f_F$, the macroscopic equivalent stress $\sigma_e \to 0$, causing numerical difficulties.

3. COMPUTATIONAL MODEL

A three-point bend fracture specimen having a span $L = 160$ mm, depth $W = 40$ mm and notch length $a = 20$ mm is considered. Due to mode I symmetry, only one half of the specimen is modelled with finite elements as shown in Fig. 1(a). This mesh comprises a total of 544 four-noded (two-dimensional plane strain) quadrilateral elements and 599 nodal points. In Fig. 1(b), the details of the refined mesh which is used near the notch tip are displayed. The initial notch diameter b_0 is 0.05 mm. At a distance $d_0 = 0.25$ mm ahead of the notch tip, a circular (cylindrical) void of diameter $a_{10} = a_{20} = 0.05$ mm is placed as shown in Fig. 1(b). The objective of this model is to simulate the interaction between a void (which has nucleated, say, around a large second phase particle or inclusion) and the

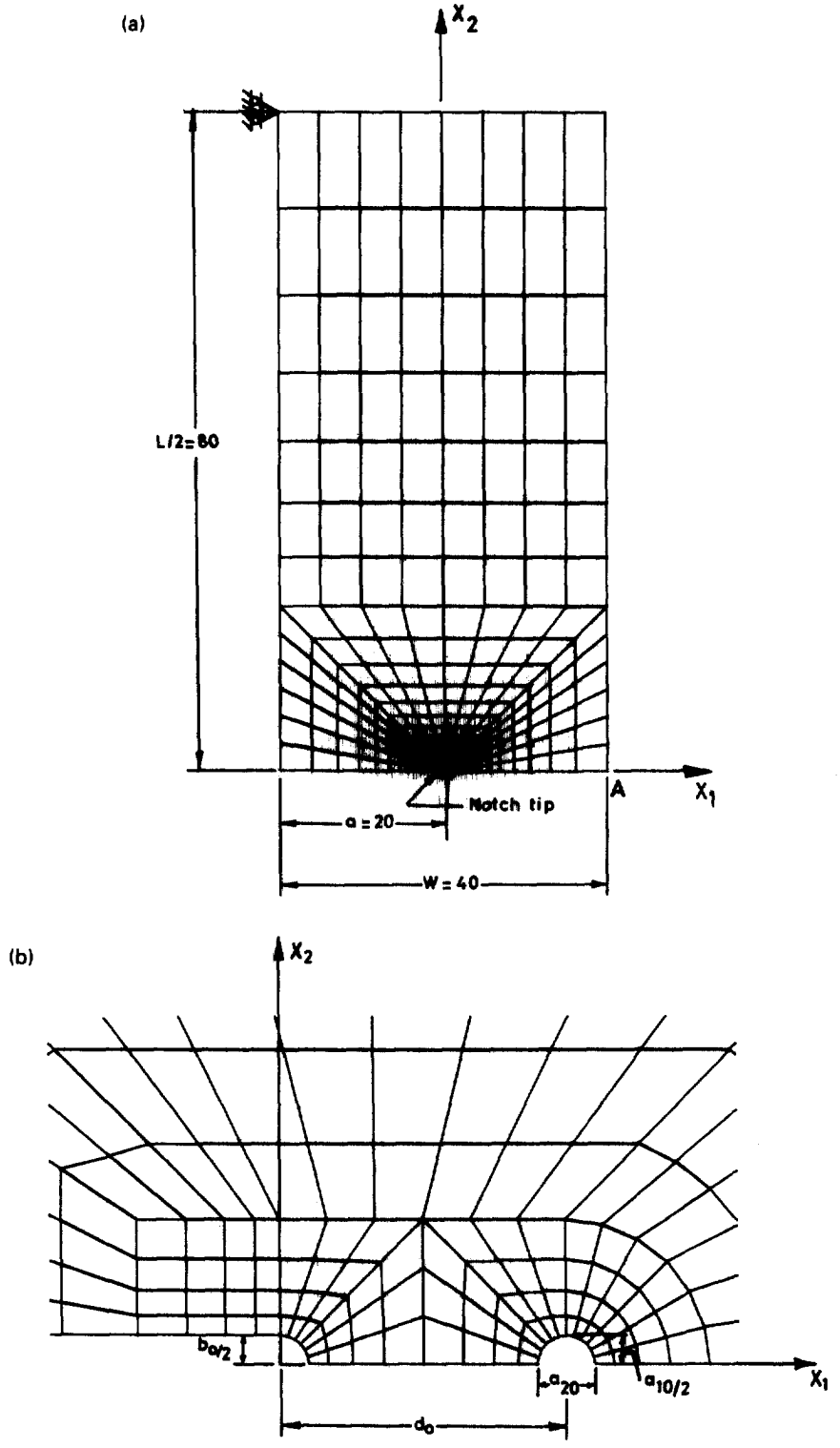

Fig. 1. (a) Mesh used in finite element analysis. All dimensions are in millimetres. (b) Details of near-tip mesh showing the notch and the hole.

notch tip under mode I static and dynamic loading. The average dimension of the smallest element (near the notch tip and hole) in Fig. 1(b) is approximately 0.012 mm.

The finite element procedure used in this work is based on an updated Lagrangian formulation that accounts for finite deformations and rotations (Narasimhan, 1994). In the mesh shown in Fig. 1(a), mode I symmetry conditions are applied on the nodes lying

along the line ahead of the notch tip ($X_2 = 0$, $X_1 > 0$). The loading of the specimen is performed by applying a specified displacement boundary condition in the negative X_1 direction at point A in Fig. 1(a). Following Needleman and Tvergaard (1991), the above specified displacement $U(t)$ at point A [see Fig. 1(a)] in all the dynamic analyses conducted here was assumed in the form:

$$U(t) = \begin{cases} V_1 t^2/(2t_1) & \text{for} \quad t \leqslant t_1 \\ V_1(t - t_1/2) & \text{for} \quad t > t_1, \end{cases} \tag{10}$$

where t_1 represents a rise time (which was taken as 10 μs) and V_1 the terminal velocity of impact. The central difference scheme was used to integrate the equation of motion in the dynamic analyses. A time step size of 1.0×10^{-9} s was employed in these analyses which was sufficient to ensure that the numerical solution remained stable. Also, the stability of the numerical solution in the dynamic analyses was monitored continuously by checking the global energy balance as suggested by Belytshko (1983) for non-linear problems.

In this work, the following analyses have been carried out using the finite element mesh depicted in Fig. 1(a).

(1) A static analysis (neglecting inertial and strain rate effects) of slow gradual loading of the three-point bend specimen.

(2) Three dynamic analyses of impact-like loading of the specimen taking into account material inertia but neglecting strain rate sensitivity, with an impact speed V_1 [see eqn (10)] of 4, 10 and 15 m s^{-1}, which will be referred to henceforth as dynamic analyses 1a, 1b and 1c, respectively.

(3) Three dynamic analyses of loading as in point (2) above but taking both inertial and strain rate sensitivity effects into consideration, with an impact speed V_1 [see eqn (10)] of 4, 10 and 15 m s^{-1}, which will be referred to in the following as dynamic analyses 2a, 2b and 2c, respectively.

The above set of analyses has been designed to yield insight into the individual as well as combined effects of material inertia and strain rate sensitivity on dynamic, ductile crack initiation. In each analysis, the computations have been conducted until all the elements in the ligament between the notch tip and the hole [see Fig. 1(b)] have experienced material failure by ductile void coalescence. This is reasonably indicative of ductile fracture initiation (Rice and Johnson, 1970; Aravas and McMeeking, 1985).

Although no attempt has been made to analyse a particular engineering material, the material properties were taken to be representative of low strength steels. The values of the material parameters used were as follows: $E = 2 \times 10^5$ N mm^{-2}, $\nu = 0.3$, $\sigma_0 = 200$ N mm^{-2}, $\dot{\varepsilon}_0 = 0.1$ and $N = 0.1$. In the static analysis and dynamic analyses 1a, 1b and 1c, the value of m was taken as 0.001. It has been found, from an analysis using a single element uniaxial model, that this value of m effectively suppresses strain rate sensitivity. A value of $m = 0.07$ was employed for dynamic analyses 2a, 2b and 2c, which fits well with the data given by Campbell and Fergusson (1970) for mild steel. The parameters used in the Gurson model were $f_n = 0.04$, $\varepsilon_n = 0.3$, $s_n = 0.1$, $f_c = 0.15$ and $f_F = 0.25$.

4. RESULTS AND DISCUSSION

As mentioned earlier, the present work has been carried out with the view of understanding the effects of material inertia and strain rate sensitivity on dynamic, ductile fracture initiation. To this end, both global and micromechanical quantities have been closely monitored and salient results will be presented below. In particular, attention will be focused on the growth of the hole ahead of the notch tip and development of porosity in the ligament due to the intense deformation field generated by the blunting of the notch.

4.1 *Deformed meshes*

The deformed meshes near the notch tip obtained from dynamic analysis 1b at $t = 109.5$ μs and $t = 127$ μs are displayed in Figs 2 and 3, respectively. At the stage

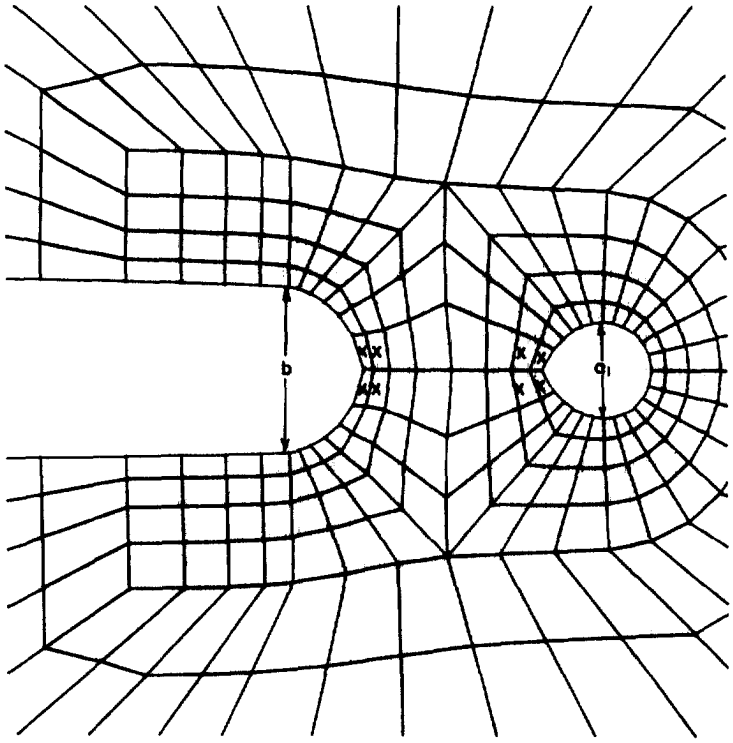

Fig. 2. Deformed mesh near the notch tip obtained from dynamic analysis 1b at time $t = 109.5$ μs. The failed elements are marked by a cross.

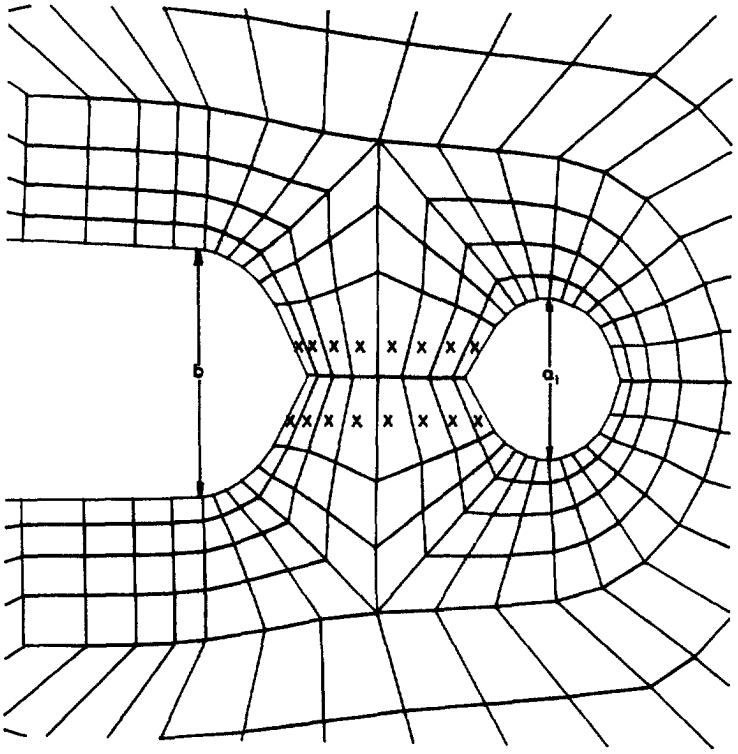

Fig. 3. Deformed mesh near the notch tip obtained from dynamic analysis 1b at time $t = 127$ μs. The failed elements are marked by a cross.

represented in Fig. 2, the notch has blunted to a diameter $b = 2.9b_0$ and the longitudinal diameter a_1 of the hole has attained a value of $1.75a_{10}$. Material failure has just initiated near the notch tip and near the hole. The elements marked by a cross in Fig. 2 have experienced failure. In other words, the void volume fraction f in these elements has attained the pre-set failure limit of $0.95f_F$ (see Section 2) or these elements have lost their stress carrying capacity.

At $t = 127$ μs to which Fig. 3 pertains, the notch diameter $b = 3.4b_0$ and the longitudinal hole diameter $a_1 = 2.2a_{10}$. At this stage, all the elements in the ligament between the notch tip and the hole which are marked by a cross have failed. This can be perceived from the large stretching and distortion undergone by these elements in Fig. 3. The qualitative features of the deformed meshes in the static analysis and in the other dynamic analyses were similar to Figs 2 and 3 and are not presented here.

4.2. *Time variation of* J

In all the analyses carried out in this work, the J integral as formulated by Eshelby (1970) for the finite deformation case, was computed at various stages of loading. For the static analysis, it was evaluated on several semicircular and rectangular contours surrounding the notch tip and was found to be almost path independent. However, for dynamic loading, J should be evaluated on a contour which is shrunk onto the crack tip [see Nakamura *et al.* (1986)]. For this purpose, a domain integral version of J proposed by Nakamura *et al.* (1986), which was appropriately modified for finite deformations, was employed to compute J from the finite element results. It should be mentioned here that for materials obeying incremental plasticity theories, J is not equal to the energy release rate. However, it is expected to serve as a measure of the intensity of the near-tip deformation fields, provided that the loading to the crack tip region is monotonically increasing and the stress histories for material particles are nearly proportional.

The time variations of J obtained from dynamic analyses 1b and 2b are shown in Fig. 4. It can be noted from this figure that J increases monotonically with time. The curves presented in Fig. 4 start with almost zero slope but steepen considerably towards the end with the development of large scale plasticity. The two curves in Fig. 4 are virtually coincident in the beginning. However, thereafter J versus time for dynamic analysis 2b, with strain rate effects added, shows a steeper climb with almost constant slope. The J versus time curve for dynamic analysis 1b, on the other hand, increases at a much slower rate.

The stage at which complete material failure due to microvoid coalescence occurred in the ligament connecting the hole with the notch tip is indicated in Fig. 4. As mentioned

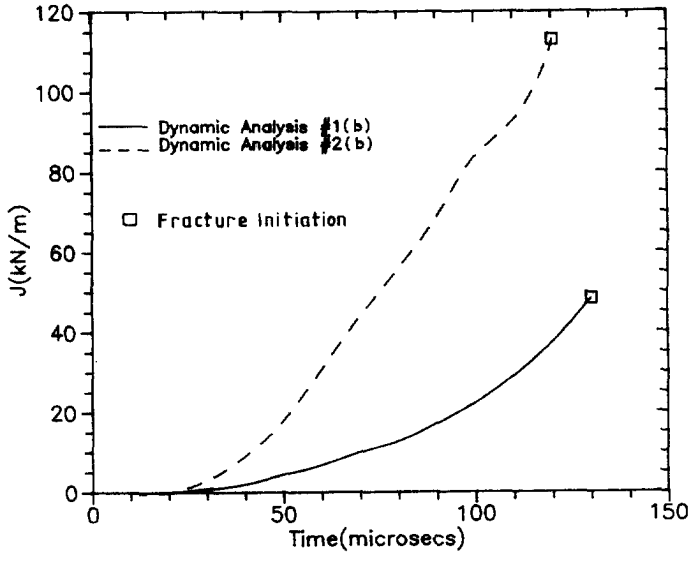

Fig. 4. Variation of the dynamic J integral with time.

in Section 3, ductile fracture initiation is assumed to have taken place at this stage. The value of J, the notch tip opening displacement and the increase in the longitudinal hole diameter, normalized by J/σ_0, at fracture initiation for all the analyses conducted here, is presented in Table 1. Also indicated in this table is the time at fracture initiation, t_f, and the rate of loading (of the near-tip region) $\dot{J} = J_f/t_f$ for the dynamic analyses. It can be seen from this table that t_f decreases with increasing impact speed for both sets of dynamic analyses. For the rate-independent material, $\dot{J}$ increases from 2.2×10^5 to 4.4×10^5 kN ms^{-1} as V_1 changes from 4 to 15 m s^{-1}. On the other hand, for the rate-dependent material, the $\dot{J}$ value is higher and varies from 3.9×10^5 to 1.1×10^6 kN ms^{-1} as V_1 increases from 4 to 15 m s^{-1}. It should further be noted that there seems to be a tendency for $\dot{J}$ to saturate at some levels as the impact speed increased beyond 10 m s^{-1}.

As has been noted by Jha and Narasimhan (1992), in the context of rate-independent material behaviour, a high value of $\dot{J}$ allows for a J-controlled field to stabilize near the notch tip in the sense that the field quantities around the tip tend to approach the variations predicted by the Hutchinson–Rice–Rosengren (HRR) analysis. Although the present analysis is different from the work of Jha and Narasimhan (1992), in the sense that plastic flow localization due to the presence of a void ahead of the notch tip is considered here, the notch tip opening displacement for the rate-independent case will be shown to compare well with the HRR analysis in Section 4.4.

On examining the values of J_f summarized in Table 1, it can be seen that it shows only a moderate increase for the rate-independent case under dynamic loading as compared with that for static loading. Thus, J_f for the static analysis and dynamic analysis 1a are almost the same, while J_f for dynamic analysis 1c is about 50% higher than the static case. On the other hand, the values of J_f for the rate-dependent material under dynamic loading are much higher than that for static loading. Indeed, J_f for dynamic analysis 2a ($\dot{J} = 3.9 \times 10^5$ kN ms^{-1}) is about 2.6 times that for the static analysis, while for dynamic analysis 2c ($\dot{J} = 1.1 \times 10^6$ kN ms^{-1}), it is 3.8 times the static value. The above results clearly indicate that while material inertia only moderately increases the critical value of J at ductile fracture initiation for the loading rate $\dot{J}$ of 10^5–10^6 kN ms^{-1} encountered in this work, strain rate sensitivity (included in dynamic analyses 2a–2c) causes a dramatic elevation in J_f. The reasons for this trend will become clear later after the results pertaining to hole growth and accumulation of micro-void damage in the ligament connecting the notch tip with the hole are analysed.

4.3. *Plastic strain localization and porosity development*

The evolution of porosity is intimately related to the development of high hydrostatic tension and to plastic strain localization. It is well known (Hutchinson, 1968) that hydrostatic tension ahead of the notch tip under mode I plane strain is very high. In the present simulations, coalescence of the void with the notch takes place via a void sheet (Cox and Low, 1974) rather than by direct impingement. Early theories, which did not consider evolution of porosity, tried to formulate approximate relations, connecting void, ligament and notch dimensions, that had to be satisfied at a point when sudden coalescence became imminent. Such relations have been proposed, for example, by Rice and Johnson (1970) and by Brown and Embury (1973). The present approach obviates the need for using such

Table 1. Values of J, normalized notch and hole opening at failure

Analysis type	J_f (kN m^{-1})	$\left(\frac{b-b_0}{J/\sigma_0}\right)$	$\left(\frac{a_1-a_{10}}{J/\sigma_0}\right)$	t_f (μs)	$\dot{J}_d$ (kN ms^{-1})
Static	34.5	0.51	0.32		
Dynamic 1a	36.0	0.50	0.32	162	2.2×10^5
Dynamic 1b	48.0	0.49	0.25	127	3.8×10^5
Dynamic 1c	52.0	0.49	0.24	118	4.4×10^5
Dynamic 2a	89.5	0.26	0.15	232	3.9×10^5
Dynamic 2b	106.0	0.21	0.13	120	8.8×10^5
Dynamic 2c	132.0	0.19	0.105	116	1.1×10^6

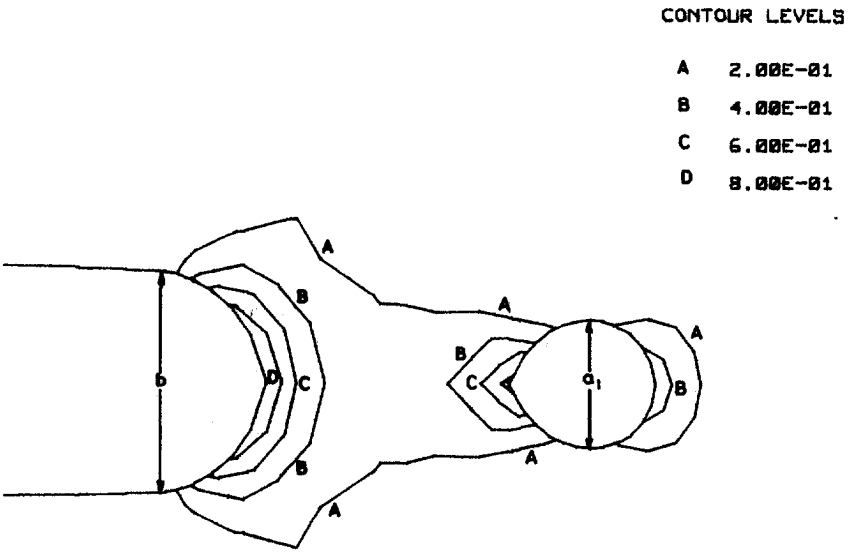

Fig. 5. Contours of the matrix plastic strain obtained from dynamic analysis 1b at $t = 109.5$ μs.

relations because phenomena like intense strain localization and consequent weakening of the ligament with development of porosity are accounted for in a natural way by the constitutive equations explained in Section 2.

The contours of matrix plastic strain ε_m^p at $t = 109.5$ μs and $t = 127$ μs obtained from dynamic analysis 1b are presented in Figs 5 and 6. These figures show the localization of plastic strain in the ligament. From Fig. 5, it can be seen that regions of high plastic strain have developed around the hole as well as the notch, while the plastic strain in the middle of the ligament is still small. Figure 6 shows that these regions of high plastic strain have moved towards each other and bridged the ligament. Thus, it is clear that the approach adopted in this work is more realistic than placing a void in the strain field of a blunting crack, because, as can be seen from Figs 5 and 6, the void makes a strong contribution towards modifying the local strain field ahead of the notch. In fact, the growth of the void and its interaction with the notch leads ultimately to plastic strain localization in the ligament as can be seen in Fig. 6.

The narrow band of plastic strain localization in the ligament in Fig. 6 causes porosity to develop inside it, while regions outside remain relatively free from porosity. In order to

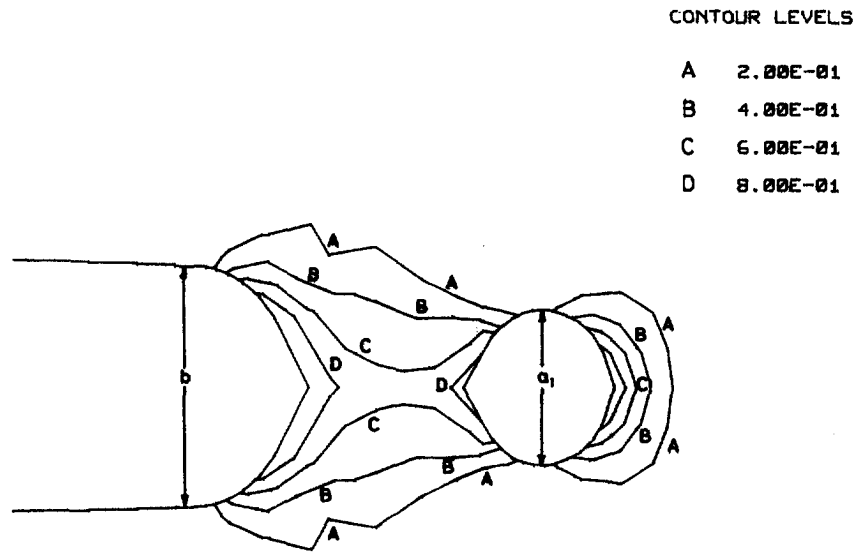

Fig. 6. Contours of matrix plastic strain obtained from dynamic analysis 1b at $t = 127$ μs.

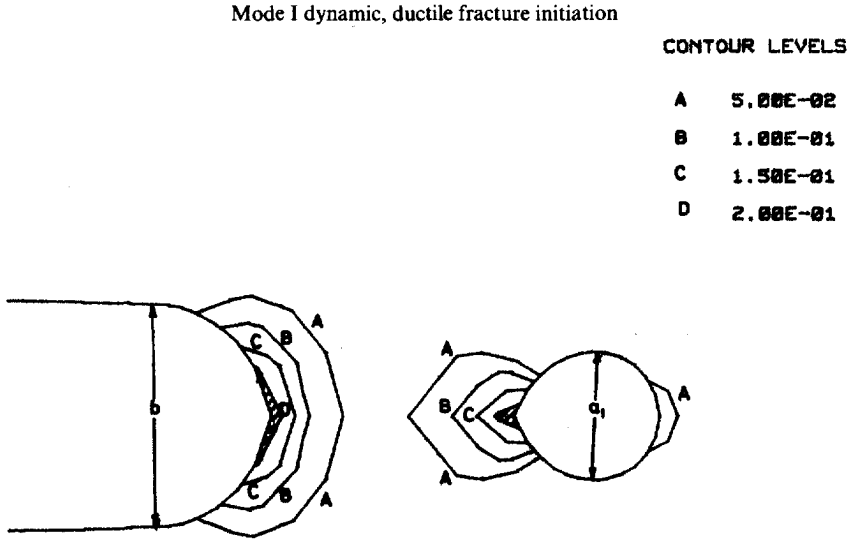

Fig. 7. Contours of void volume fraction obtained from dynamic analysis 1b at $t = 127$ μs. The hatched region represents microvoid damage zone.

understand this, the contours of void volume fraction f at $t = 109.5$ and 127 μs obtained from dynamic analysis 1b are displayed in Figs 7 and 8. It can be observed from Fig. 7 that there is a high level of porosity formation near the notch tip and hole, while the value of f in the middle of the ligament is much smaller. In other words, contours of void volume fraction near the hole spread back towards the notch, while those near the notch spread forward towards the hole.

The accumulation of porosity near the notch and the hole in Fig. 7 has been caused by large plastic strain concentration (compare Fig. 7 with Fig. 5) and high triaxiality. The regions within contour D (shown hatched in Fig. 7) have experienced material failure (i.e. $f \simeq 0.95 f_F$). In other words, these are regions which have lost their stress carrying capacity. They can be treated as an extension of either the void or the crack, depending upon their points of emanation. On comparing Fig. 7 with Fig. 2, it can be seen that the failed elements (marked by a cross in Fig. 2) are within the microvoid damage zones which are shown hatched in Fig. 7.

At $t = 127$ μs, it can be observed from Fig. 8 that the contours of high void volume fraction from the hole and the notch have linked up with each other. The region within contour D shown hatched in Fig. 8, which encompasses the entire ligament between the

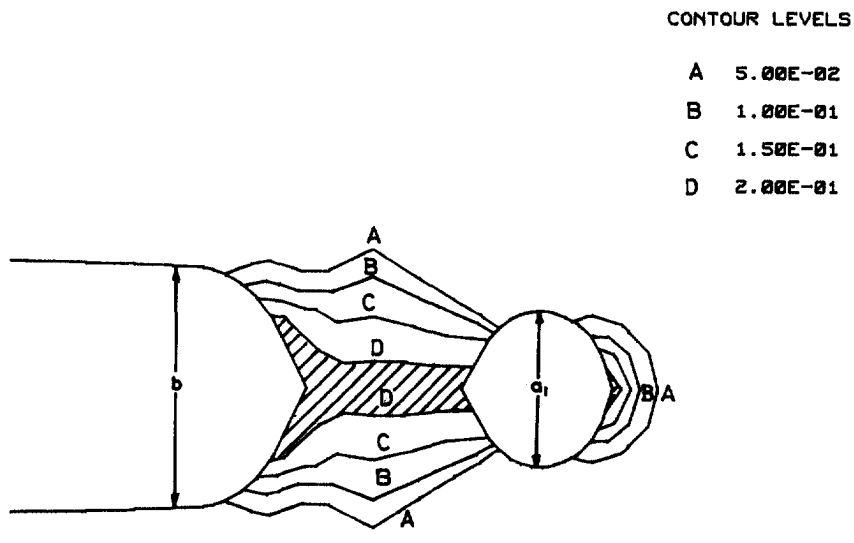

Fig. 8. Contours of void volume fraction obtained from dynamic analysis 1b at $t = 127$ μs. The hatched region represents microvoid damage zone.

notch and the hole, has experienced material failure by micro-void damage. This was already noted in connection with the deformed mesh presented in Fig. 3 (see elements marked by a cross in Fig. 3).

There is a strong similarity between the contours of matrix plastic strain shown in Figs 5 and 6 and those of void volume fraction displayed in Figs 7 and 8. At $t = 109.5$ μs, the central portion of the ligament (within contour A in Fig. 5) begins to undergo plastic strain controlled void nucleation. This leads to rapid failure of the ligament at around $t = 127$ μs as can be seen from Fig. 8. The above phenomenon corresponds to the classic void sheet mechanism, which has been observed in experimental studies [see, for example, Cox and Low (1974)] involving materials with two sets of void nucleating particles of vastly different sizes.

The hatched region in Fig. 8, within which failure by void sheeting has taken place, is a narrow band that bridges the entire ligament between the notch tip and the hole. It should be noted here that concentrations of void volume fraction contours encircling discrete points (representing the small scale particles) within this band are not perceived in Fig. 8. This is because, as mentioned in Section 2, the small scale particles (which are, conceivably, less than 1 μm in size) are assumed to be uniformly dispersed in the matrix. An explicit modelling of a statistically significant number of these tiny particles, in a manner such that their discrete character is preserved, would require an extremely fine discretization with its consequent implication on the computational requirements. However, the important physical processes of strain concentration in the ligament after the notch and hole have deformed to some extent and its consequent failure by porosity formation, which are involved in void sheeting, are well represented in the present simulations. This is a direct outcome of the use of the Gurson constitutive equations [in particular, the micro-void nucleation law, eqns (6) and (7)].

Figures 9–11 show the progressive development of failure by microvoid coalescence in the ligament between the notch tip and the hole for the static analysis and dynamic analyses 1b and 2b, respectively. This is depicted in the variations of the void volume fraction with distance along the ligament measured in the undeformed configuration for different values of the normalized (near-tip) loading parameter $J/(\sigma_0 a_{10})$. In interpreting these figures it should be noted that the notch tip is located at $X_1 = 0.025$ mm and the hole end at $X_1 = 0.225$ mm in the undeformed configuration. Further, it should be recalled from Section 2 that the pre-set failure limit for f is $0.95 f_F$, which is equal to 0.2375. It can be seen from these figures that in the case of the static analysis (Fig. 9) and dynamic analysis 1b (Fig. 10) micro-void damage accumulation in the ligament develops in a qualitatively similar

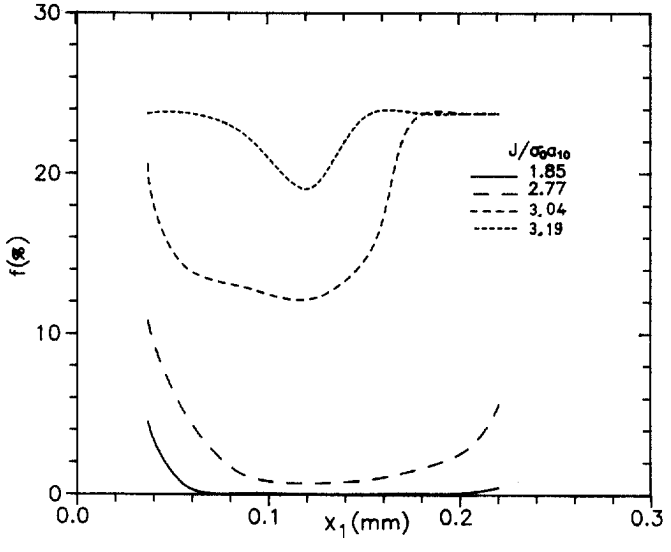

Fig. 9. Variation of f along the ligament connecting the notch and the hole obtained from the static analysis for different J values.

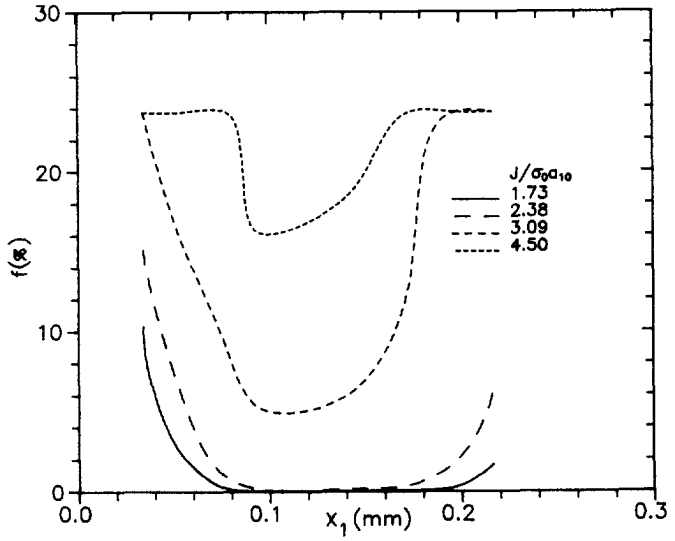

Fig. 10. Variation of f along the ligament connecting the notch and the hole obtained from the dynamic analysis 1b for different J values.

way. In these cases, material failure progresses first from the hole and subsequently also from the notch tip, and the two failure zones meet somewhere in the middle of the ligament. This feature was also typical of dynamic analyses 1a and 1c involving the rate-independent material. The value of J at fracture initiation (i.e. when the entire ligament fails) for dynamic analysis 1b is moderately higher than that for the static analysis, as noted earlier, and is attributed to material inertia.

Failure development in dynamic analysis 2b (Fig. 11) shows a departure from the trends seen in the two previous figures. At lower values of J, the value of f at the notch tip is higher than at the hole end. This is because higher plastic strains near the notch tip have led to early void nucleation in this region; but it can be observed from Fig. 11 that, at higher values of J, f near the hole becomes higher than that near the notch tip and failure, unlike in the two previous cases, proceeds predominantly from the hole towards the notch tip. The tremendous rise in flow stresses encountered in this analysis gives rise to a high hydrostatic tensile stress in the ligament. As the peak value of the hydrostatic stress is attained at some finite distance ahead of the notch tip, the hole end is a preferred site for

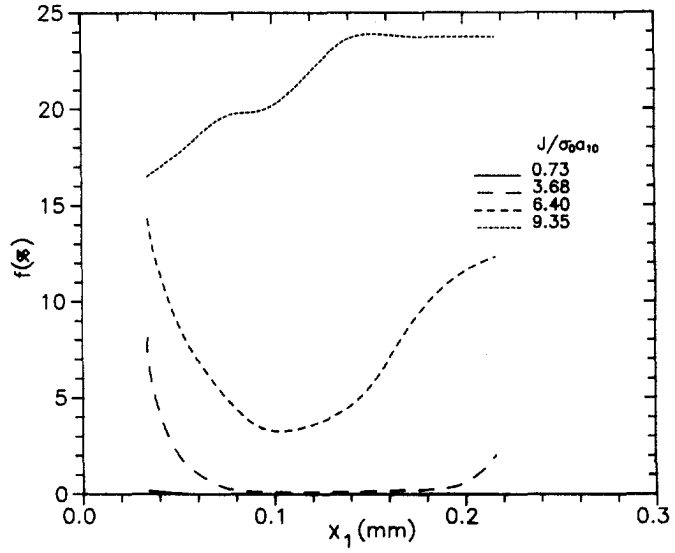

Fig. 11. Variation of f along the ligament connecting the notch and the hole obtained from the dynamic analysis 2b for different J values.

porosity development at later stages of deformation. Also, it should be noted on comparing Fig. 11 with Figs 9 and 10 that the value of $J/(\sigma_0 a_{10})$ to attain comparable levels of void volume fraction in the ligament is much higher for dynamic analysis 2b as compared with the static analysis and dynamic analysis 1b. Consequently, as seen in Table 1, the value of J at fracture initiation for dynamic analyses 2a–2c is also much higher than the corresponding value in the static analysis and dynamic analyses 1a–1c.

4.4. *Notch opening and hole growth*

In Fig. 12, the variation of the normalized notch tip opening displacement $(b-b_0)/a_{10}$ with respect to the normalized (near-tip) loading parameter $J/(\sigma_0 a_{10})$ is presented. The results obtained from the static analysis and from dynamic analyses 1b and 2b are compared in these figures. It can be observed from the figure that the variation of the notch tip opening displacement with $J/(\sigma_0 a_{10})$ computed from the static analysis and dynamic analysis 1b (rate-independent case) are almost identical until the point of fracture initiation. In fact, both these curves in Fig. 12 match closely the variation predicted by the asymptotic HRR (Hutchinson, 1968) analysis and also the work of Shih (1981) based on the J_2 flow theory of plasticity, which is given by $b-b_0 \sim d_n J/\sigma_0$, where $d_n = 0.47$ for $n = 10$ and $\sigma_0/E = 0.001$. This was also true for dynamic analyses 1a and 1c, as can be seen from the ratios $(b-b_0)/(J/\sigma_0)$ at failure that are summarized in Table 1. The above result corroborates observations made in previous studies [see, for example, Jha and Narasimhan (1992)] that an HRR type field which is characterized uniquely by J is established near the notch tip in the region surrounding the fracture process zone where ductile void coalescence occurs.

On the other hand, it can be seen from Fig. 12 that in dynamic analysis 2b, which has taken into account rate sensitivity, the notch tip opening increases at a much slower rate with $J/(\sigma_0 a_{10})$ compared with the other two curves. This is attributed to the local flow stress elevation due to strain rate effects near the notch tip in dynamic analysis 2b. Indeed, it is known from the results of Shih (1981) that the parameter $d_n = (b-b_0)/(J/\sigma_0)$ decreases with increasing strain hardening. Now, on referring to Table 1, it can be seen that the above ratio at fracture initiation for dynamic analyses 2a–2c is much lower than that for the rate-independent material and is in the range 0.26–0.19.

The increase in the longitudinal hole diameter normalized by the initial hole diameter, $(a_1-a_{10})/a_{10}$, is plotted against $J/(\sigma_0 a_{10})$ in Fig. 13. Again, in the interest of clarity, only results pertaining to the static analysis and dynamic analyses 1b and 2b are presented in this figure. It can be seen from the figure that the static analysis leads to the fastest growth rate of the hole with respect of J, followed by dynamic analysis 1b. Dynamic analysis 2b,

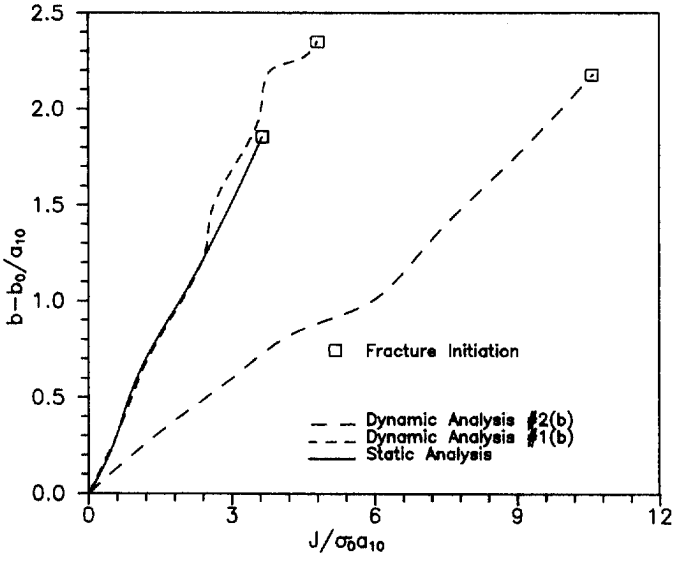

Fig. 12. Variation of normalized notch tip opening displacement versus $J/(\sigma_0 a_{10})$. Comparison between the static and two dynamic analyses.

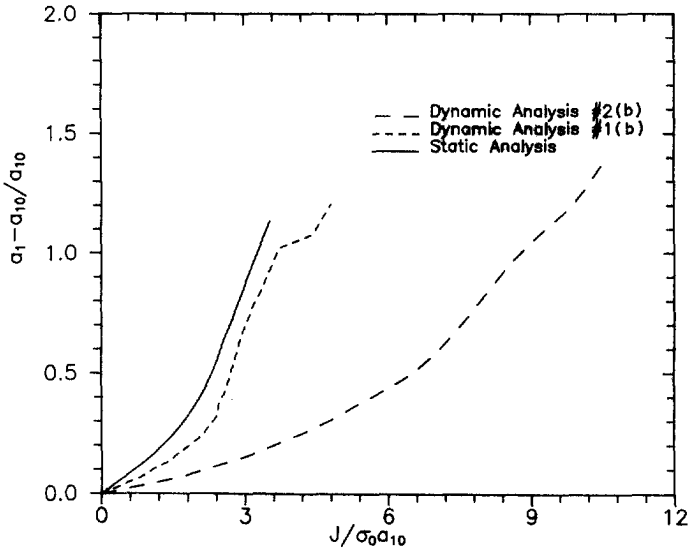

Fig. 13. Change in longitudinal hole diameter normalized by a_{10} versus $J/(\sigma_0 a_{10})$. Comparison between the static and two dynamic analyses.

which incorporates strain rate sensitivity, shows the slowest growth rate. For example, to attain a current hole diameter of $a_1 = 2a_{10}$, the value of $J/(\sigma_0 a_{10})$ in the static analysis is 3.3, while it is 3.7 and 8.8 in the two dynamic analyses, respectively. In fact, the void growth rate (with respect of J) for all the dynamic analyses involving the rate-dependent material was much slower than that for the dynamic analyses involving the rate-independent material. Indeed, it can be observed from Table 1 that the (non-dimensional) ratio $(a_1 - a_{10})/(J/\sigma_0)$ at fracture initiation is in the range 0.32–0.24 for dynamic analyses 1a–1c. The decrease in this ratio with increase in impact velocity is clearly an outcome of inertial effects operating inside the plastic zone. On the other hand, the above ratio is much lower and falls in the range 0.15–0.105 for dynamic analyses 2a–2c. In this case, the reduction in this ratio as V_1 increases (and also in comparison with the static case) is attributed to the combined effect of strain rate sensitivity and material inertia. Clearly, the role played by the former is more pronounced as can be seen by comparing the above ratio for dynamic analysis 2a with the static value.

Thus, for the loading rate considered in this work ($\dot{J} \sim 10^5$–10^6 kN ms^{-1}), the effect of material inertia in decreasing the growth rate (with respect to J) of a hole situated near the notch tip is marginal. On the other hand, flow stress elevation due to high plastic strain rates experienced by the material around the hole under dynamic loading significantly retards the growth of the hole. As already observed in connection with Figs 9–11, it also dramatically slows down the accumulation of micro-void damage in the ligament between the notch tip and the hole. The above result is similar to the observation made by Thomason (1990) about the effect of strain hardening on the growth of a spherical void in a rigid plastic material. He has found, based on an approximate integration of the Rice and Tracey (1969) equations, that the presence of strain hardening reduces the void growth rates and this effect is more dramatic at higher hydrostatic stress levels. Further support for the present results can be found from the work of Budiyansky *et al.* (1982) on the growth of a spherical void in a non-linearly viscous solid which follows a uniaxial relation similar to eqn (8). It can be clearly observed from Fig. 5.1(a,b) of their paper that the dilatation rate of a spherical void decreases as the rate exponent m increases and this effect is more pronounced at higher hydrostatic stress levels.

It should be noted here that the present study does not model nucleation of a large discrete void around an inclusion (by, say, debonding), but instead assumes the presence of a pre-nucleated hole near the notch tip. It is to be expected that flow stress elevation due to strain rate sensitivity will promote early void nucleation, since the critical stress required to trigger debonding at the matrix–particle interface will be attained earlier. Indeed, this

has been observed in the simulations of Narasimhan and Kamat (1994) who accounted for the presence of a distribution of large second phase particles in an approximate manner, within the framework of the Gurson model. In such a situation, the diameter of the (nucleated) hole for the rate-dependent case may not show as dramatic a difference from the rate-independent case as in Fig. 13 based on the present study. Further, as observed by Narasimhan and Kamat (1994), thermal softening caused by adiabatic heating near the notch tip under dynamic loading will have the opposite effect of rate sensitivity and will accelerate the growth of a void. However, Narasimhan and Kamat (1994) found that for a loading rate similar to that encountered in this work ($\dot{J} \sim 5 \times 10^5$ kN ms^{-1}), adiabatic heating did not play as great a role as rate sensitivity. In fact, the steel considered in their work had very high strength ($\sigma_0 = 1000$ N mm^{-2}) and a peak temperature rise of around 300°C near the notch tip was computed from their dynamic analysis.

5. CONCLUSIONS

In this work, two-dimensional (plane strain) finite element analyses of a three-point bend specimen subjected to both quasi-static and dynamic loading have been conducted. The interaction between a pre-nucleated hole and the notch tip in the above process has been studied. The important conclusions of the work are summarized below.

(1) Ductile fracture in the present simulations has been found to occur by the classic void sheet mechanism due to concentration of intense plastic strain in the ligament connecting the notch tip and the hole.

(2) Strain rate sensitivity significantly delays the development of ductile failure (with respect to the fracture characterizing parameter J) under dynamic loading in the following ways: (a) retards the growth of a hole near the notch tip; (b) retards the opening of the notch; and (c) considerably slows down the rate of accumulation of micro-void damage in the ligament between the notch tip and a nearby hole.

(3) Both material inertia and strain rate sensitivity are found to play a beneficial role on dynamic, ductile fracture initiation in the sense that they elevate the value of J at fracture initiation. However, while the influence of the former is moderate, for the loading rate of $\dot{J} \sim 10^5$ kN ms^{-1} encountered in this work, the latter has a very strong effect on the failure process.

It should be noted, however, that factors like stress controlled void nucleation at large size inclusions and thermal softening (due to adiabatic heating) may also have important contributions towards causing or impeding ductile fracture initiation.

REFERENCES

Andersson, H. (1977). Analysis of a model for void growth and coalescence ahead of a moving crack tip. *J. Mech. Phys. Solids* **25**, 217–233.

Aoki, S., Kishimoto, K., Takeya, A. and Sakata, M. (1984). Effects of microvoids on crack blunting and initiation in a ductile material. *Int. J. Fracture* **24**, 267–278.

Aravas, N. and McMeeking, R. M. (1985). Microvoid growth and failure in the ligament between a hole and a blunt crack tip. *Int. J. Fracture* **29**, 21–38.

Argon, A. S., Im, J. and Safoglu, R. (1975). Cavity formation from inclusions in ductile fracture. *Metall. Trans.* **6A**, 825–837.

Belytshko, T. (1981). An overview of semidiscretization and time integration procedures. In *Computational Methods for Transient Analysis* (Edited by T. Belytshko and T. J. R. Huges), pp. 1–65. North-Holland, Amsterdam.

Benson, D. J. (1993). An analysis of void distribution effects on the dynamic growth and coalescence of voids in ductile metals. *J. Mech. Phys. Solids* **41**, 1285–1308.

Brown, L. M. and Embury, J. D. (1973). Initiation and growth of voids at second phase particles. In *Proceedings of the Third International Conference on Strength of Metals and Alloys*, pp. 164–179. Institute of Metals, London.

Budiyansky, B., Hutchinson, J. W. and Slutsky, S. (1982). Void growth and collapse in viscous solids. In *Mechanics of Solids* (Edited by H. G. Hopkins and M. J. Sewell), pp. 13–45. Pergamon Press, Oxford.

Campbell, J. D. and Fergusson, W. G. (1970). The temperature and strain rate dependence of the shear strength of mild steel. *Phil. Mag.* **21**, 63–82.

Chu, C. C. and Needleman, A. (1980). Void nucleation effects in biaxially stretched sheets. *J. Engng Mater. Technol.* **102**, 249–256.

Cox, T. B. and Low, J. R. (1974). An investigation of the plastic fracture of AISI 4340 and 18Ni-200 grade maraging steels. *Metall. Trans.* **5**, 1457–1470.

Eshelby, J. D. (1970). The energy momentum tensor in continuum mechanics. In *Inelastic Behaviour of Solids* (Edited by M. F. Kanninen, W. F. Adler, A. R. Rosenfield and R. I. Jaffe), pp. 77–114. McGraw-Hill, New York.

Gurson, A. L. (1977). Continuum theory of ductile rupture by void nucleation and growth—Part I. *J. Engng Mater. Technol.* **99,** 2–15.

Hutchinson, J. W. (1968). Singular behaviour at the end of a tensile crack in a hardening material. *J. Mech. Phys. Solids* **16,** 13–31.

Jha, M. and Narasimhan, R. (1992). A finite element analysis of dynamic fracture initiation by ductile failure mechanism in a 4340 steel. *Int. J. Fracture* **56,** 209–231.

McMeeking, R. M. (1977). Finite deformation analysis of crack-tip opening in elastic–plastic materials and implications for fracture. *J. Mech. Phys. Solids* **25,** 357–381.

Nakamura, T., Shih, C. F. and Freund, L. B. (1986). Analysis of a dynamically loaded three-point bend ductile fracture specimen. *Engng Fracture Mech.* **25,** 323–339.

Narasimhan, R. (1994). A numerical study of static and dynamic fracture initiation in a ductile material containing a dual population of second phase particles. *Engng Fracture Mech.* **47,** 919–948.

Narasimhan, R. and Kamat, S. V. (1994). A numerical investigation of ductile fracture initiation in a high strength low-alloy steel. *Bull. Mater. Sci.* **17,** 259–282.

Needleman, A. and Tvergaard, V. (1987). An analysis of ductile rupture modes at a crack tip. *J. Mech. Phys. Solids* **15,** 151–185.

Needleman, A. and Tvergaard, V. (1991). An analysis of dynamic, ductile crack growth in a double edged specimen. *Int. J. Fracture* **49,** 41–67.

Pan, J., Saje, M. and Needleman, A. (1983). Localisation of deformation in rate sensitive porous plastic solids. *Int. J. Fracture* **21,** 261–278.

Pierce, D., Shih, C. F. and Needleman, A. (1984). A tangent modulus method for rate dependent solids. *Comput. Structures* **18,** 875–887.

Priest, A. H. (1976). Influence of strain rate and temperature on the fracture and tensile properties of several metallic materials. In *Proceedings of the International Conference on Dynamic Fracture Toughness*, pp. 95–111. Welding Institute, Cambridge.

Rice, J. R. and Johnson, M. A. (1970). The role of large geometry changes in plane strain fracture. In *Inelastic Behaviour of Solids* (Edited by M.-F. Kanninen, A. R. Adler, A. R. Rosenfield and R. I. Jaffe), pp. 641–672. McGraw-Hill, New York.

Rice, J. R. and Tracey, D. M. (1969). On the ductile enlargement of voids in tri-axial stress fields. *J. Mech. Phys. Solids* **17,** 201–217.

Shih, C. F. (1981). Relationship between *J*-integral and the crack opening displacement for stationary and extending cracks. *J. Mech. Phys. Solids* **29,** 305–326.

Thomason, P. F. (1990). *Ductile Fracture of Metals.* Pergamon Press, Oxford.

Tvergaard, V. (1981). Influence of voids on shear band instabilities under plane-strain conditions. *Int. J. Fracture* **17,** 389–407.

Tvergaard, V. (1982). On localization in ductile materials containing spherical voids. *Int. J. Fracture* **18,** 237–252.

Tvergaard, V. and Needleman, A. (1984). Analysis of cup-cone fracture in a round tensile bar. *Acta Metall.* **32,** 157–169.

Tvergaard, V. and Needleman, A. (1988). An analysis of temperature and rate dependence of Charpy V-notch energies for a high nitrogen steel. *Int. J. Fracture* **37,** 197–215.